60 GHz WIRELESS LINKS FOR HDTV: CHANNEL CHARACTERIZATION AND ERROR PERFORMANCE EVALUATION

Andreas G. Siamarou[1, *], Panagiotis Theofilakos[2], and Athanasios G. Kanatas[2]

[1]School of Computing and Mathematics, University of Central Lancashire, Cyprus, 12–14 University Avenue, Pyla, Larnaka 7080, Cyprus

[2]Department of Digital Systems, University of Piraeus, 80 Karaoli and Dimitriou st., Piraeus, Attiki 185 34, Greece

Abstract—This paper presents results from an indoor LOS channel measurement campaign at the 60 GHz band. The results include the Ricean K-factor and time dispersion/frequency selectivity characteristics, which dominate the data-rate and error-performance limitations of the channel. Finally, three clusters are identified and the well known Saleh-Valenzuela model is used to statistically describe the interarrival times and the power decay of clusters and multipath components in the clusters.

1. INTRODUCTION

Broadband wireless local area networks earmarked for future multimedia services in the 60-GHz band envisage data transmission rates of up to 15 Gb/s [1–3]. Examples of applications include very high speed Internet access, streaming content download, uncompressed high definition distribution, Video on Demand, Video Coding Transmission, High Definition Television (HDTV), future home networks, home theatre, real-time streaming, high capacity data storage and High-Definition Multimedia Interface (HDMI) for cable replacement. HDTV and the ultra high-definition video are leading a revolution of home entertainment experience, as people are going to be surrounded by

high capacity multimedia devices. The establishment of 60-GHz multi-gigabit links between these devices will enable the easy and quick delivery of high-definition content and will eliminate the need for compression.

In this paper, the indoor channel characteristics are investigated for the 60-GHz band, using measured data in a typical large room environment.

2. MEASUREMENT SETUP

2.1. Hardware Setup

The wideband channel sounder used for channel characterization is presented in [4]. At the transmitter, the VNA (HP8714C)-synthesized output is swept in steps between 1 and 2 GHz and then upconverted in frequency (mixed) to a 62.4 GHz carrier prior to transmission. An external 100 MHz oven-controlled crystal (OVC) was used as a reference for both phase-locked oscillators (PLOs) used at the transmit and receive units. The upconverter has an IF bandwidth from DC to 6 GHz. The output of the upconverter consists of two sidebands at a level approximately 6–7 dB below the swept IF signal level. The upper sideband with frequencies between 63.4 and 64.4 GHz is passed through a bandpass filter centered at 64.4 GHz. The bandpass filter also suppresses the lower sideband between 60.4 and 61.4 GHz. The level of suppression (rejection band) is specified as > 20 dB. At the receiver, a 62.4 GHz PLO is synthesized from the same 100-MHz OVC by connecting a very-low-loss 50 m Sucoflex flexible coaxial cable from the transmitter to the receiver. The cable-specified loss is 0.23–0.73 dB/m. The phase coherence between the transmitter and receiver enables the phase information to be retrieved. The 1- to 2-GHz signal is coherently detected, amplified by an LNA with a bandwidth of 900–2000 MHz and 32 dB gain, and then fed back through a second 50 m Sucoflex flexible coaxial cable to the receive port of the VNA. This allows the measurement of the wireless channel complex transfer function (CTF). The dynamic range of the system was estimated to be 70 dB with a noise floor of -110 dBm. The frequency resolution of the measurement system was 625 kHz, since 1601 frequency tones were transmitted in a bandwidth of 1 GHz. The bandwidth of the measurement system was limited by the bandwidth of the LNA used at the receiver. The corresponding time resolution is 1nsec and the maximum measured excess delay is 1600 nsec. The hardware setup is illustrated on Fig. 1 [4].
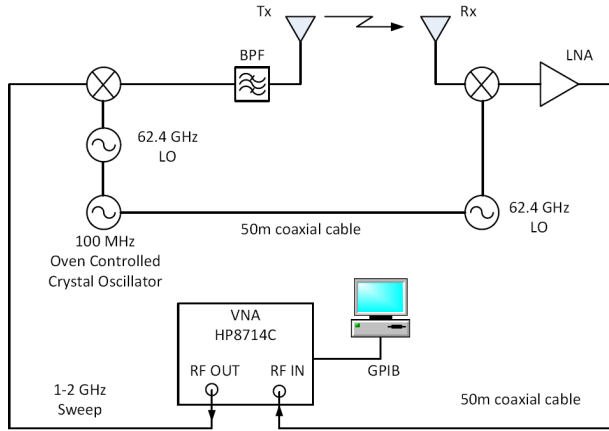
Figure 1. Illustration of the hardware setup.

2.2. Calibration Procedure

Prior to measurements, equipment and cables calibration was performed inside an anechoic chamber in order to extract their influence from the measured data. Since the VNA measured the transfer function of the radio channel, it was necessary to remove the antenna effects and calculate the propagation channel transfer function for further analysis. The transmitter employs a standard horn antenna with a gain of $10\,$dBi and $69°$ and $55°$ $3\,$dB beamwidths for the E and H-plane respectively. An omnidirectional antenna of $6\,$dBi gain and elevation beamwidth of $6.5°$ is used at the receiver end. The measured radio channel transfer function is given by

$$H_{\mathrm{radio}}(f) = \sum_{i=1}^{1601} S_{21}^{\mathrm{meas}}(f_i)\,\delta(f - f_i), \quad f_1 \leq f \leq f_{1601}, \qquad (1)$$

where $S_{21}^{\mathrm{meas}}(f_i)$ is the measured S_{21} parameter by the VNA at frequency tone f_i. This function includes the effects of both the propagation channel and the transfer functions of the transmitting and receiving antennas, i.e.,

$$H_{\mathrm{radio}}(f) = H_{\mathrm{prop}}(f)\,H_{\mathrm{ant}}(f), \qquad (2)$$

where $H_{\mathrm{prop}}(f)$ is the desired CTF, and $H_{\mathrm{ant}}(f)$ denotes the combined transfer function of the antennas utilized. This function was measured following the procedure described in [5, 6] as

$$H_{\mathrm{ant}}(f) = \frac{S_{21}(f)}{H_{\mathrm{fs}}(f)}, \qquad (3)$$

where $S_{21}(f)$ is the VNA recording in the anechoic chamber,

$$H_{\text{fs}}(f) = \frac{\lambda}{4\pi d_0} e^{-j\frac{2\pi}{\lambda}d_0} \qquad (4)$$

is the free space transfer function, and d_0 is the reference distance of the measurement.

2.3. HDTV Measurement Scenario

The environment under test is typical indoor, i.e., a small room in a relatively new building type, with thick walls made of bricks and concrete blocks [4], depicted in Fig. 2. The floor was carpeted, and the ceiling was covered with polystyrene tiles. This room contained electric metallic heaters, was cubically shaped, and also contained windows together with a metal fire door and two white display boards on one of the walls. The furniture in the room were removed to allow channel characterization based on the reflections produced by the superstructure of the environment. The room dimensions are $12.80\,\text{m} \times 6.92\,\text{m} \times 2.60\,\text{m}$, which is an excellent scenario for HDTV and HDMI. The antennas were placed at a height of $1.7\,\text{m}$ above the floor level and pointing at each other's direction. Static measurements were taken on the room diagonal with a spatial sampling of $30\,\text{cm}$, starting from a position with $1.5\,\text{m}$ transmitter-receiver separation. A total of thirty-eight LOS channel transfer function measurements were recorded within the room that correspond to a maximum transmitter-receiver range of $12.80\,\text{m}$. For noise reduction purposes, each recording is the result of averaging of eight VNA frequency sweeps.
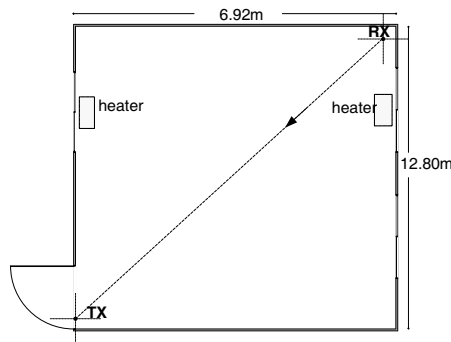

Figure 2. A model of the environment under test.

3. MEASUREMENT RESULTS

The main objective of the propagation measurements is to determine the error-rate and data-rate limitations. Error performance in an indoor LOS scenario is dominated by the so-called Ricean K-factor and data rate is limited by the frequency selectivity of the channel. In this section, we explore these characteristics based on our measurements and apply the Saleh-Valenzuela model to describe the clustering of the multipath components.

3.1. Ricean K-factor

Small scale fading in LOS scenarios, the fading amplitude r_n at the n-th time instant can be represented as $r_n = \sqrt{(x_n + \beta)^2 + y_n^2}$, where β is the amplitude of the specular (LOS) component and x_n, y_n are zero-mean Gaussian random variables with variance σ^2. The Ricean K-factor is defined as the ratio of specular to defused energy [7, 8], i.e.,

$$K = \frac{\beta^2}{2\sigma^2}. \tag{5}$$

K-factor is an important channel parameter, as it determines the error performance of digital communications links over Ricean channels. The estimated K-factors versus transmitter-receiver distance in our measurement scenario are depicted in Fig. 3. As observed, the K-factor ranges from approximately $0.5\,\mathrm{dB}$ to $11\,\mathrm{dB}$ with a trend to decrease with increasing distance.
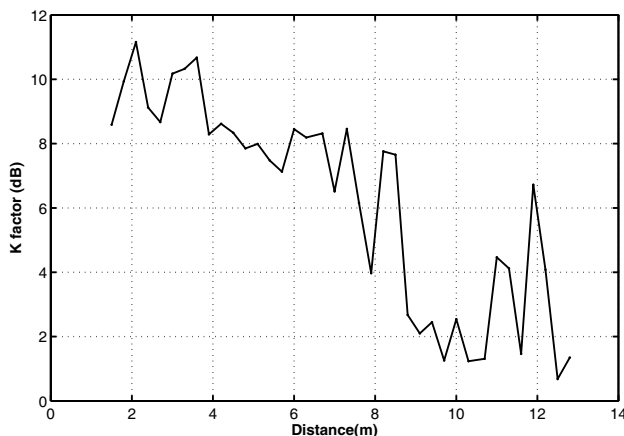

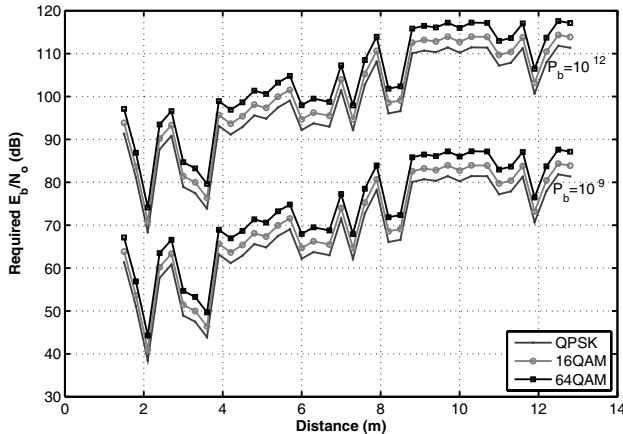**Figure 3.** Ricean K-factor versus distance.

Figure 4. Required average E_b/N_o to achieve a target bit error probability of 10^{-9} and 10^{-12}.

3.2. Error Performance

Uncompressed HD streaming applications require stringent restrictions on error probability to ensure high quality video. Therefore, rather than presenting the bit error rate performance, it is more meaningful to calculate the required bit energy over noise ratio (E_b/N_0) versus transmitter-receiver distance to achieve a rather low target error probability, such as 10^{-9} and 10^{-12}.

To avoid tedious computer simulations, the uncoded bit error probability of QPSK and M-ary QAM over Ricean fading channels is evaluated theoretically, using a moments-generating-function (MGF) approach presented in [9]. As the K-factor for a fixed transmitter-receiver distance has already been calculated, bit error probability can be easily evaluated for any E_b/N_0 value. Thus, the required E_b/N_0 to achieve a target bit error probability can be easily evaluated using numerical methods.

As shown in Fig. 4, a target error probability of 10^{-12} can be achieved when E_b/N_0 is approximately 120 dB, if 64QAM is used. Of course, the required E_b/N_0 will be reduced significantly by channel coding and using aligned antennas with high directivity.

3.3. Time Dispersion Parameters

Frequency selectivity (and thus limitations on achievable data rates) is determined by the time dispersion of the channel. Time dispersion modeling is based on the power delay profile (PDP), which is

constructed by the complex baseband channel impulse response (CIR). The CIR was calculated by inverse Fourier transform (IFFT) of the measured CTF. First, the CIR was normalized to its maximum value; then, the PDP was calculated as $P(\tau, d_l) = |h(\tau, d_l)|^2$, $l = 1, \ldots, 38$. Next, the multipath with the maximum power was identified and located at the origin of the delay axis, whereas all multipaths were normalized in power with respect to the first component. The time dispersion parameters were calculated for all transmitter-receiver distances. The calculation was based on the PDPs after applying a threshold value of $-50\,\text{dB}$ with respect to the strongest multipath. All multipaths with power lower than the threshold value were discarded. The threshold value limits the maximum excess delay and determines the length of the cyclic prefix in an OFDM based system. The mean excess delay $\bar{\tau}$, is defined as the first moment of PDP. The r.m.s. delay spread τ_{rms}, is the square root of the second central moment of PDP [11], i.e.,

$$\tau_{rms} = \sqrt{\overline{\tau^2} - (\bar{\tau})^2}, \tag{6}$$

$$\overline{\tau^n} = \frac{\sum\limits_i P(\tau_i)\tau_i^n}{\sum\limits_i P(\tau_i)}, \quad n = 1, 2. \tag{7}$$

Figs. 5 and 6 show the variation of r.m.s. delay spread and mean excess delay respectively versus transmitter-receiver distance. It is easily observed that the r.m.s. delay spread ranges from 36 ns to 50 ns, whereas the mean excess delay ranges from 5 ns to 9.2 ns.
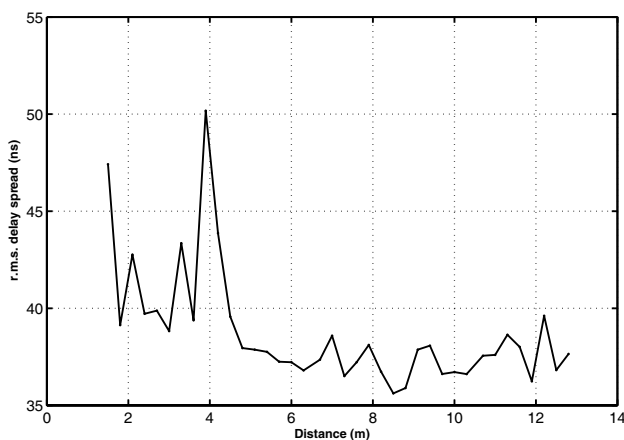

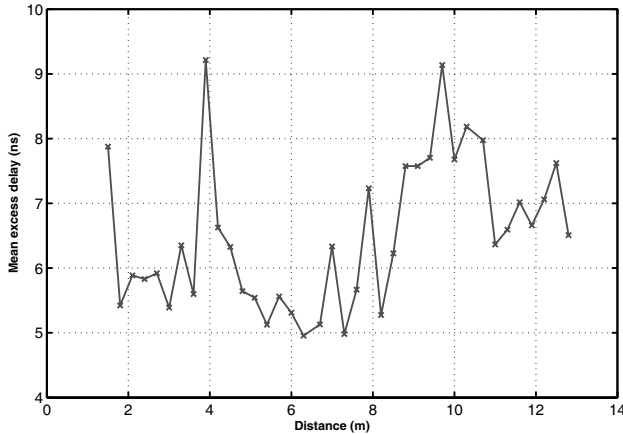**Figure 5.** R.m.s delay spread versus distance.

Figure 6. Mean excess delay versus distance.

3.4. Coherence Bandwidth

Another commonly used measure of the frequency-selectivity of a wireless channel is the coherence bandwidth B_c. This bandwidth defines the difference in frequency required so that the value of the frequency correlation function is smaller than a given threshold. The coherence bandwidth for a correlation threshold c, can be evaluated as [10]

$$B_c = \arg\min\left\{\Delta f > 0 : |R_H(\Delta f)| = c\right\}, \tag{8}$$

where $R_H(\Delta f)$ is the normalized frequency correlation function of the channel, given by the Fourier transform of the PDP, i.e.,

$$R_H(\Delta f) = \int_0^{\tau_{\max}} P(\tau) e^{-j2\pi\Delta f\tau} d\tau. \tag{9}$$

The $c = 0.9$ coherence bandwidth of the channel versus transmitter-receiver distance ranges from 10 MHz to approximately 90 MHz and is depicted in Fig. 7. It is clearly observed that the coherence bandwidth preserves a fluctuation with distance similar to that of the r.m.s. delay spread.

3.5. Saleh-Valenzuela Model Parameters

The well-known Saleh-Valenzuela (S-V) model [11] was selected to describe the clustering of the multipath components. A single PDP was used for the S-V model parameter extraction that was calculated as an average of local PDPs measured at several distances in the room.
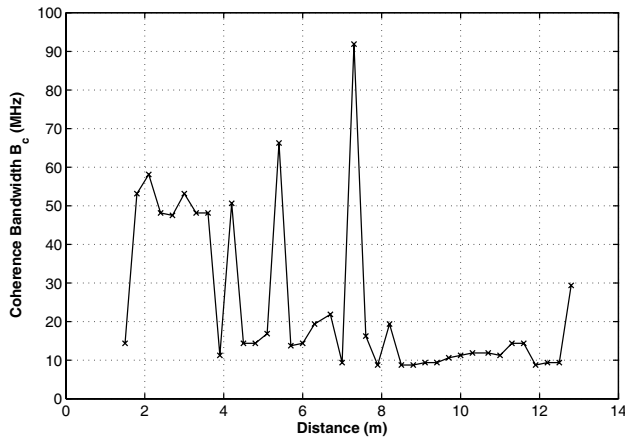
Figure 7. Coherence bandwidth for $c = 0.9$ versus distance.

This profile is called henceforth APDP and is depicted in Fig. 8. Three clusters of multipath components are clearly observed. According to the S-V model, the cluster inter-arrival time as well as the rays inter-arrival time within a cluster are described by independent exponential probability density functions (pdf) and the important parameters are the mean cluster arrival rate Λ and the mean ray arrival rate λ. The value of cluster arrival rate $1/\Lambda$ was found to be 386 nsec. Since the regularly spaced ray arrival times model is adopted in this work, the ray arrival rate is equal to the delay bin duration i.e., $\lambda = 1$ nsec. Having identified the clusters one may calculate the decay exponent of the clusters, Γ, and the rays in the clusters, γ. The Γ value is determined from the corresponding best fit regression lines of the first multipath component amplitude of each cluster. The decay factor is calculated as $\Gamma = \frac{10}{m_\Gamma \ln 10}$, where m_Γ is the negative slope of the regression line on the dB scale. The estimated value of the cluster exponential decay factor Γ was 71.81 ns. In order to calculate the decay exponent γ of the rays the values of the normalized power of the rays and their relative delays were superimposed and plotted. Then, following the same method described for the estimation of Γ the decay exponent of the rays was estimated as $\gamma = \frac{10}{m_\gamma \ln 10}$, where m_γ is the negative slope of the regression line on the dB scale. The estimated value of the ray exponential decay factor γ was 19.48 ns. Fig. 8 also presents the power decay slope of the clusters and the corresponding rays, based on the estimated values.
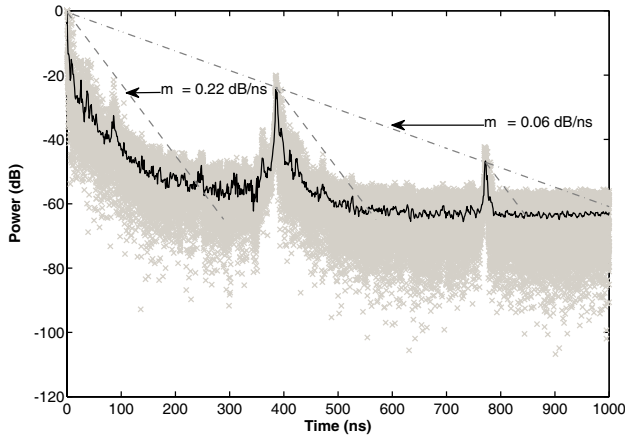
Figure 8. Average power delay profile.

4. CONCLUSION

Measurement results of a 60 GHz indoor LOS wideband channel have been presented. The variability of Ricean K-factor and time delay spread with transmitter-receiver distance has been studied. The required bit energy over noise ratio to achieve a predefined bit error probability has been evaluated. The uncoded bit error probability of QPSK and M-ary QAM over Ricean fading channels has been evaluated theoretically, using MGF approach. For 64QAM and for a target error probability of 10^{-12}, the required E_b/N_0 is approximately 120 dB. This threshold value can be reduced significantly by channel coding and using aligned antennas with high directivity. The investigation of the delay spread in the channel provided a maximum r.m.s. delay spread of 50 ns and a maximum mean excess delay of 9.2 ns. The coherence bandwidth was calculated in order to characterize the frequency-selectivity of the channel and provided values ranging from 10 MHz to 90 MHz. Finally, the channel has been modeled by using the Saleh-Valenzuela model. The cluster arrival rate was found to be 386 nsec. The estimated value of the cluster exponential decay factor Γ was 71.81 ns, whereas the rays exponential decay factor γ was 19.48 ns.

REFERENCES

1. Siamarou, A. G., "Broadband wireless local-area networks at millimeter waves around 60 GHz," *IEEE Antennas Propag. Mag.*, Vol. 45, No. 1, 177–181, Feb. 2003.

2. Smulders, P., "Exploiting the 60 GHz band for local wireless multimedia access: Prospects and future directions," *IEEE Commun. Mag.*, Vol. 40, No. 1, 140–147, Jan. 2002.

3. Daniels, R. C. and R. W. Heath, Jr., "60 GHz wireless communications: Emerging requirements and design recommendations," *IEEE Trans. Veh. Technol.*, Vol. 2, No. 3, 41–50, Mar. 2007.

4. Siamarou, A. G. and M. O. Al-Nuaimi, "A wideband frequency domain channel sounding system and delay spread measurements at the licence free 57–64 GHz band," *IEEE Trans. Instrum. Meas.*, Vol. 59, No. 3, 519–526, Mar. 2010.

5. Promwong, S., W. Hachitani, and J.-I. Takada, "Free space link budget evaluation of UWB-IR systems," *Proc. International Workshop on Ultra Wideband Systems*, 312–316, May 2004.

6. Spiliotopoulos, C. G. and A. G. Kanatas, "Channel measurements and modelling in a military cargo airplane," *Progress In Electromagnetics Research B*, Vol. 26, 69–100, 2010.

7. Tepedelenlioglu, C., A. Abdi, and G. B. Giannakis, "The Ricean K factor: Estimation and performance analysis," *IEEE Trans. Wireless Commun.*, Vol. 2, No. 4, 799–810, Jul. 2003.

8. Greenstein, L. J., S. S. Ghassemzadeh, V. Erceg, and D. G. Michelson, "Ricean K-factors in narrow-band fixed wireless channels: Theory, experiments and statistical models," *IEEE Trans. Vehic. Techn.*, Vol. 58, No. 8, 4000–4012, Oct. 2009.

9. Alouini, M.-S. and A. J. Goldsmith, "A unified approach for calculating error rates of linearly modulated signals over generalized fading channels," *IEEE Trans. Commun.*, Vol. 47, No. 9, 1324–1334, Sep. 1999.

10. Fleury, B. H., "First- and second-order characterization of direction dispersion and space selectivity in the radio channel," *IEEE Trans. Info. Theory*, Vol. 46, No. 6, 2027–2044, Sep. 2000.

11. Saleh, A. and R. A. Valenzuela, "A statistical model for indoor multipath propagation," *IEEE J. Sel. Areas Commun.*, Vol. 5, No. 2, 128–137, Feb. 1987.